Journal of Alloys and Compounds xxx (2013) xxx–xxx

Contents lists available at ScienceDirect

Journal of Alloys and Compounds

journal homepage: www.elsevier.com/locate/jalcom

Structural evolution upon decomposition of the $LiAlH_4 + LiBH_4$ system

S. Soru [a], A. Taras [a], C. Pistidda [b], C. Milanese [c], C. Bonatto Minella [d], E. Masolo [a], P. Nolis [g], M.D. Baró [e], A. Marini [c], M. Tolkiehn [f], M. Dornheim [b], S. Enzo [a], G. Mulas [a], S. Garroni [a,*]

[a] Department of Chemistry and Pharmacy, University di Sassari and INSTM, Via Vienna 2, I-07100 Sassari, Italy
[b] Institute of Materials Research, Materials Technology, Helmholtz-Zentrum Geesthacht, Max-Planck, Str. 1, D-21502 Geesthacht, Germany
[c] Pavia H2 Lab, C.S.G.I. & Dipartimento di Chimica, Sezione di Chimica Fisica, Università di Pavia, Viale Taramelli 16, I-27100 Pavia, Italy
[d] IFW Dresden, Institute for Metallic Materials, Helmholtzstrasse 20, D-01069 Dresden, Germany
[e] Universitat Autònoma de Barcelona, Departament de Física, E-08193 Bellaterra, Spain
[f] DESY Synchrotron, Beam Line D3, Hamburg, Germany
[g] Servei de Ressonància Magnètica Nuclear and Departament de Química, Universitat Autònoma de Barcelona, E-08193 Bellaterra, Spain

ARTICLE INFO

Article history:
Available online xxxx

Keywords:
Hydrogen storage materials
$LiBH_4$
Synchrotron Radiation Powder X-ray Diffraction
Solid State Magic Angle Spinning (MAS) Nuclear Magnetic Resonance (NMR)

ABSTRACT

In the present work we focus the attention on the phase structural transformations occurring upon the desorption process of the $LiBH_4 + LiAlH_4$ system. This study is conducted by means of manometric–calorimetric, *in situ* Synchrotron Radiation Powder X-ray Diffraction (SR-PXD) and *ex situ* Solid State Magic Angle Spinning (MAS) Nuclear Magnetic Resonance (NMR) measurements. The desorption reaction is characterized by two main dehydrogenation steps starting at 320 and 380 °C, respectively. The first step corresponds to the decomposition of $LiAlH_4$ into Al and H_2 *via* the formation of Li_3AlH_6 whereas the second one refers to the dehydrogenation of $LiBH_4$ (molten state). In the range 328–380 °C, the molten $LiBH_4$ reacts with metallic Al releasing hydrogen and forming an unidentified phase which appears to be an important intermediate for the desorption mechanism of $LiBH_4$–Al-based systems. Interestingly, NMR studies indicate that the unknown intermediate is stable up to 400 °C and it is mainly composed of Li, B, Al and H. In addition, the NMR measurements of the annealed powders (400 °C) confirm that the desorption reaction of the $LiBH_4 + Al$ system proceeds *via* an amorphous boron compound.

1. Introduction

In the field of the hydrogen-based fuel cells technology, enormous efforts have been devoted to the development of materials capable to reversibly store high amounts of hydrogen with favorable thermodynamic and kinetic properties [1–3]. Currently, large interest is addressed towards a class of materials defined as tetraborohydrides, due to their high gravimetric hydrogen storage densities [4]. Among them, $LiBH_4$ is considered one of the most attractive and promising materials for automotive application, because of its high hydrogen gravimetric capacity of 18.5 wt.% [2,5,6]. However, due to its high thermodynamic stability (T_{des} > 500 °C) and sluggish sorption kinetics, $LiBH_4$ does not meet the requirements set for on-board hydrogen storage [7]. Recently, in order to tailor the thermodynamics and the kinetics of $LiBH_4$ de-hydrogenation process, different approaches were proposed which can be classified in three categories: the addition of catalysts, the nanoconfinement into scaffolds and the destabilization of the tetrahydroborate by combination with a hydride phase.

Doping with several additives including halides, oxides and pure metals effectively reduces the dehydriding temperature of $LiBH_4$ [8–12]. For example, Au et al. verified that the halides TiF_3, $TiCl_3$ and $ZnCl_2$, when added to $LiBH_4$, form unstable transition metal borohydride species which contribute to drastically reduce the thermal desorption temperature of the doped $LiBH_4$ from 300 °C to less than 100 °C [9]. Destabilization of $LiBH_4$ was also achieved by the addition of different oxides with the following order of efficiency: $Fe_2O_3 > V_2O_5 > Nb_2O_5 > TiO_2 > SiO_2$ [10]. More recently, Pendolino and coauthors demonstrated that the desorption temperature of $LiBH_4$ can be decreased from 500 °C to 350 °C by the addition of boron [12].

Another method is represented by the confinement of $LiBH_4$ in mesoporous scaffolds, nanotubes and carbon aerogels [13–17]. $LiBH_4$ was successfully infiltrated into the mesoporous channels of SBA-15 under hydrogen pressure [13]. For the as-prepared $LiBH_4$/SBA-15 nanocomposite, the initial desorption temperature was 150 °C [14]. Vajo et al. reported that fast desorption kinetics of $LiBH_4$ was achieved (50 times at 300 °C) when it was confined within a nanoporous carbon scaffold. However, despite recent progress, the employment of scaffolds drastically decreases the hydrogen storage density of the whole system.

* Corresponding author. Tel.: +39 079 229524; fax: +39 079 229559.
E-mail address: sgarroni@uniss.it (S. Garroni).

0925-8388/$ - see front matter © 2013 Elsevier B.V. All rights reserved.
http://dx.doi.org/10.1016/j.jallcom.2013.12.027

The third approach concerns with the opportunity to tailor the thermodynamic properties of complex hydrides by incorporating a second or a third compound in the reacting mixture to stabilize the reaction products [18–23]. Bösenberg et al. mixed $LiBH_4$ and MgH_2 aiming to modify the thermodynamics for the de/rehydrogenation process of $LiBH_4$. By this approach, MgB_2 is formed during dehydrogenation [24]. The $LiBH_4/MgH_2$ composite system decomposes at lower temperature compared to pure $LiBH_4$ and good reversibility was achieved under milder conditions. Fichtner et al. prepared, by ball milling, a TiF_3-doped $LiBH_4$–$LiAlH_4$ (2:1) mixture that starts to decompose between 177 and 247 °C and can reversibly absorb hydrogen up to 5.1 wt.% [25]. In addition, Pressure–Composition–Temperature (PCT) experiments pointed out a reduction of the decomposition enthalpy of $LiBH_4$ from 74 kJ/mol H_2 (pristine $LiBH_4$) to 60.4 kJ/mol H_2 for the TiF_3-doped composite system [26]. More recently, Walker et al. demonstrated that the destabilization of $LiBH_4$, induced by a synergic effect of Ti and $LiAlH_4$, can be improved by longer milling times of the starting materials [27]. Nevertheless, despite the long list of works on the $LiBH_4/LiAlH_4$ system, up to our knowledge, no experimental investigation is reported for the nominal stoichiometry 1:1.

In this study, the desorption reaction for the binary $LiBH_4$–$LiAlH_4$ (1:1) composite system has been investigated in detail by means of combining manometric–calorimetric measurements, *in situ* Synchrotron Radiation Powder X-ray Diffraction (SR-PXD) and *ex situ* solid-state MAS Nuclear Magnetic Resonance (NMR).

2. Experimental details

Commercial powders of $LiBH_4$ (95% purity) and $LiAlH_4$ (97% purity) were purchased from Sigma–Aldrich and Alfa Aesar, respectively. The binary mixture of $LiBH_4$–$LiAlH_4$ in a molar ratio 1:1 was prepared by high-energy ball milling using a Spex Mix mod. 8000. 5 g of powders were sealed in a stainless steel vial and the milling was performed under argon atmosphere with 2 balls (10 g each one), for 30 h with a rotation speed of 875 rotation per minute, rpm. The powders were manipulated inside a glove box (MBraun-20-G) with high-purity argon atmosphere and O_2 and H_2O levels below 0.1 ppm.

Structural evolution of the milled powders was characterized by means of *in situ* Synchrotron Radiation Powder X-ray Diffraction (SR-PXD), performed at the beamline D3 of the HASYLAB, DESY, Hamburg. A high-pressure sample cell provided with a sapphire capillary and specifically designed for *in situ* monitoring of solid/gas reactions was used [24]. The *in situ* measurement was performed at 1 bar of Ar pressure. The powders were heated from 30 to 400 °C with 5 °C/min as heating rate and then kept for 40 min at 400 °C. Each X-ray diffraction (XRD) pattern was collected with an exposure time of 30 s using a wavelength (λ) of 0.49902 angstrom (Å). The FIT2D program was used to convert the two dimensional images into the one dimensional powder patterns [28]. Phase abundance and microstructural parameters were evaluated by fitting the XRD patterns by Rietveld method with the software MAUD [29].

Coupled manometric–calorimetric measurements were performed on the as-milled powders: a high-pressure cell of Sensys DSC (Setaram) was charged with 50 mg of powder under Ar atmosphere in a glove box and was directly connected to the manometric instrument (PCTPro-2000 by Setaram & Hy-Energy; pressure sensors accuracy: 1% of reading) by a 1/8″ stainless steel tube. Thermal programmed desorption steps (TPD) were performed by heating the samples from room temperature to 450 °C at 5 °C/min under an atmosphere of 0.5 bar of hydrogen.

Solid-state Magic Angle Spinning (MAS) Nuclear Magnetic Resonance (NMR) spectra were recorded using a Bruker Advance 400 MHz spectrometer with a wide bore 9.4 T magnet and by employing a boron-free Bruker 4 mm CPMAS probe. The spectral frequencies were 128.33 MHz for the ^{11}B nucleus, 155.33 for the ^{7}Li nucleus and 104.28 for the ^{27}Al nucleus. The NMR chemical shifts were reported in parts per million (ppm) externally referenced to $BF_3{\cdot}O(CH_2CH_3)_2$, LiCl and $Al(NO_3)_3$, respectively. The powder materials were packed into 4 mm ZrO_2 rotors in an argon-filled glove box and were sealed with tight fitting Kel-F caps. MAS experiments were performed at room temperature at sample rotation frequencies of 12 kHz using dry nitrogen gas. Spectra were acquired at 20 °C and the temperature was controlled by a BRUKER BCU unit.

3. Results and discussion

The coupled manometric–calorimetric profile recorded on the as-milled sample is reported in Fig. 1. The manometric analysis of the reacting $LiBH_4$–$LiAlH_4$ mixture reveals a multistep desorption path: the first desorption step starts at ca. 120 °C with a release of about 3.9 wt.% of H_2 while the second step takes places at 380 °C and corresponds to a release of 2.9 wt.% of H_2. Full dehydrogenation is not achieved at 430 °C. At this temperature, 6.8 wt.% H_2 is measured which does not match the theoretical gravimetric capacity of the system (10.12 wt.%) associated with the following reaction:

$$LiBH_4 + LiAlH_4 \rightarrow 1/2\,AlB_2 + 2LiH + 1/2\,Al + 3H_2(g) \quad (1)$$

The composite shows a complex calorimetric profile. The measurement, reported in Fig. 1 (black solid line), reveals six thermal events during heating: five endothermic peaks with onset temperature of 95 °C (A), 114 °C (B), 183 °C (D), 271 °C (E) and 380 °C (F) and one exothermic peak at 120 °C (C).

In order to further investigate the desorption reaction, *in situ* SR-PXD was performed on the $LiBH_4$–$LiAlH_4$ mixture using the same experimental conditions applied for the coupled manometric–calorimetric analysis.

Fig. 2 shows a series of XRD patterns collected in the range of temperature between room temperature and 400 °C with 5 °C/min as heating rate while Fig. 3 displays the patterns, with Rietveld fitting profiles, relevant to samples thermally treated at the temperature of the peaks in the DSC analysis. At room temperature, reflections of the starting material correspond to the *o*-$LiBH_4$ and $LiAlH_4$ are visible. Small traces of metallic Al (<4 wt.%) are also

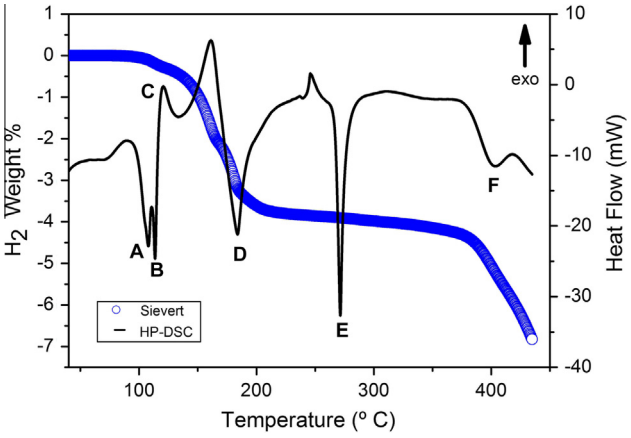

Fig. 1. Coupled manometric–calorimetric profiles acquired on the $LiBH_4 + LiAlH_4$ mixture milled for 30 h. Manometric signal: blue circles. DSC profile: black solid line. (For interpretation of the references to color in this figure legend, the reader is referred to the web version of this article.)

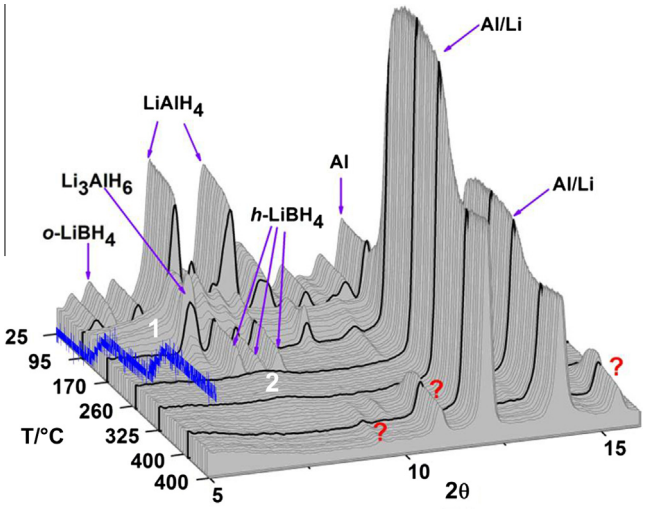

Fig. 2. In situ SR-PXD measurements of the $LiBH_4 + LiAlH_4$ mixture (3D plot). The analysis was carried out under 1 bar of Ar, heating the material from RT to 400 °C (5 °C/min) and then keeping it for 40 min under isothermal conditions at 400 °C. The blue line, depicted in perspective, represents the pressure variation monitored inside the cell during the thermal treatment. (For interpretation of the references to color in this figure legend, the reader is referred to the web version of this article.)

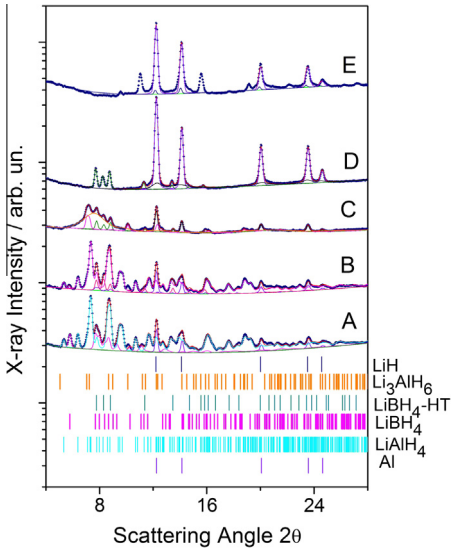

Fig. 3. In situ SR-PXD patterns of the mixture collected at the temperature of 30 °C (A), 95 °C (B), 115 °C (C), 223 °C (D) and 400 °C (E) during heating. Dots profiles are experimental data, full red lines are from the Rietveld fit. The bars at the bottom indicate the line positions expected for each phase appearing in the various examined patterns. (For interpretation of the references to colour in this figure legend, the reader is referred to the web version of this article.)

identified (see also Fig. 3A). The presence of Al is ascribable to the already existing impurity in the as-received $LiAlH_4$.

Around 95 °C *o*-$LiBH_4$ transforms (event A in Fig. 1) into the hexagonal high-temperature *h*-$LiBH_4$ polymorph (see details in Fig. 3B). The event at 115 °C (peak B in Fig. 1) corresponds to the melting reaction of $LiAlH_4$. Then, according to the manometric measurement, the significant release of gas is related to the reactions corresponding to C, D and F peaks, even confirming a multi-step desorption pathway. As a matter of fact, as the temperature reaches 115 °C the intensity of the crystalline peaks, belonging to $LiAlH_4$, decreases. At the same time, the intensity referring to the background (denoted **1** in Fig. 2) increases and the formation of Li_3AlH_6, takes place (event C in Fig. 1). The formation of Li_3AlH_6 is confirmed by the Rietveld refinement of the pattern collected at 115 °C (Fig. 3C). This result suggests that $LiAlH_4$ melts and subsequently exothermally decomposes to Li_3AlH_6, Al and H_2. Observation of these two characteristic events (peaks B and C in Fig. 1) is in according with previous works, which reported that the as-received $LiAlH_4$ melts around 170 °C (endothermic event) and quickly decomposes (exothermic event) to Li_3AlH_6 at 194 °C. The onset thermal events are shifted to lower temperatures for the milled material [30,31]. The decomposition of $LiAlH_4$ to Li_3AlH_6 is also endorsed by a sharp intensification of the diffraction peaks of Al (Fig. 2) and a slight increase of the pressure inside the cell (blue line in Fig. 2) associated to hydrogen release during this step. This is in agreement with the first desorption step at about 120 °C (Fig. 1).

Around 170 °C, the Bragg reflections related to Li_3AlH_6 start to disappear followed by an increase of the cell pressure and a further growth of intensity of the Al peaks. As reported in literature [32], Li_3AlH_6 decomposes forming LiH, Al and hydrogen. However, since Al and LiH crystallize in the same space group (*Fm-3m*) and with similar unit cell parameters (4.0494 Å and 4.0609 Å, respectively), their diffraction peaks overlap, making complicate both the qualitative and quantitative evaluation of the phases. The Al/LiH and *h*-$LiBH_4$ phases still exist over 223 °C (Fig. 3D) and, in particular, the intensity of the Al/LiH reflections increases significantly over this temperature, as shown in Fig. 2. Note that $LiBH_4$ does not seem to influence the $LiAlH_4$ decomposition step. In fact, the amount of hydrogen released during the first step (3.9 wt.% H_2 – Fig. 1) is close to the theoretical hydrogen storage capacity of $LiAlH_4$ in the whole system (5.06 wt.% H_2), if decomposes to LiH, Al and H_2 (as proved by XRD measurements).

At ca. 262 °C *h*-$LiBH_4$ starts to melt and its diffraction peaks vanish, given rise to a diffuse halo shown in Fig. 2 in the region marked as **2**. According to the literature [33], the melting occurs without evolution of hydrogen and it is characterized by an endothermic event which is confirmed by the DSC analysis reported in Fig. 1 (peak E).

Around 328 °C, the intensities of the Al/LiH peaks decrease and some signals belonging to an unknown phase show up. The formation of the unknown phase is accompanied by an increase of the pressure inside the cell, therefore the reaction between Al and molten $LiBH_4$ leads to release of hydrogen at temperature lower than pristine $LiBH_4$. The unidentified phase (denoted by the symbol **?** in Fig. 2) is stable up to 400 °C as evidenced by pattern E in Fig. 3. At this temperature, four distinct peaks show up: d_{obs} = 2.601 Å (I_{obs} = 100), 1.844 Å (I_{obs} = 87), 1620 Å (I_{obs} = 57), 1502 Å (I_{obs} = 66). Similar indexation was found by Ravnsbaek et al. for an identified phase formed at 390 °C during the thermal desorption of the $LiBH_4$ + Al (1:1.5) system [34]. More recently, Jensen et al. reported that the decomposition of the $LiBH_4$ + Al system occurs *via* two intermediate compounds observed below 500 °C which could be a new phase mainly composed by Li–Al–B species [35].

At the end of the annealing process (T = 400 °C), only the Al/LiH and the unknown phase are observed in the patterns, as emerged by Fig. 3E. In addition, no traces of AlB_2 are visible.

The as-annealed powders were then characterized by solid-state MAS NMR technique to identify the unknown specie. In Fig. 4A, ^7Li {^1H} (dark line) NMR spectrum of the mixture treated at 400 °C is displayed. A sharp peak at 0.5 ppm is observed which cannot be directly associated to LiH (+1.5 ppm). In addition, chemical shift of +19.4 ppm is measured, in accordance with the typical chemical shift of LiAl [36]. Note that the broadening of the center-band line width of LiAl suggests that the size of the LiAl crystals is very small and its integrated signal is less than 5% close to the XRD detectable limits. Regarding ^{27}Al {^1H} measurement, the pattern is reported in Fig. 4B. More than half of the observed ^{27}Al signal is due

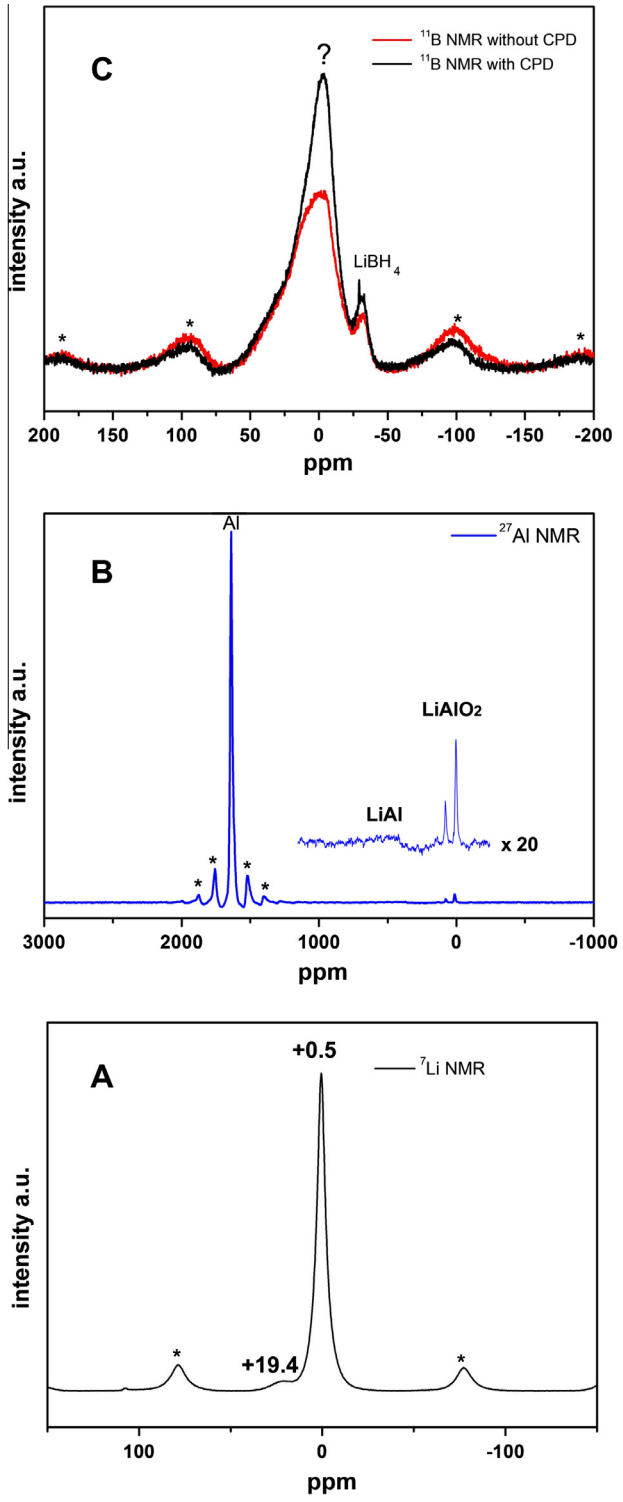

Fig. 4. (**A**) ^{7}Li {^{1}H} (dark line) (12 kHz) single-pulse NMR spectrum of the $LiBH_4 + LiAlH_4$ mixture annealed at 400 °C for 1 h. (**B**) ^{27}Al {^{1}H} (blue line) MAS (12 kHz) single-pulse NMR spectrum of the $LiBH_4 + LiAlH_4$ mixture annealed at 400 °C for 1 h. (**C**) ^{11}B {^{1}H} (dark line) and ^{11}B (red line) MAS (12 kHz) single-pulse NMR spectra of the $LiBH_4 + LiAlH_4$ mixture annealed at 400 °C for 1 h. The abbreviation ^{11}B instead of ^{11}B{^{1}H}, indicates a typical Boron NMR experiment conducted without a composite-pulse decoupling (CPD) signal. Spinning side bands are marked with an asterisk (*). (For interpretation of the references to color in this figure legend, the reader is referred to the web version of this article.)

to Al metal (1640 ppm), confirming that aluminum is the major product of the mixture annealed at 400 °C. The broad peak at ~+400 ppm and the doublet at +11.9 and +77.7 ppm (inset in Fig. 4B) can be attributed to Al nucleus in the LiAl and $LiAlO_2$ phases, respectively. In Fig. 4C, ^{11}B {^{1}H} (dark line) and ^{11}B (red line) MAS NMR spectra are shown. Residual $LiBH_4$ is detected at −37 ppm (signal 5.6%), whereas the broad peak centered around 0 ppm results difficult to assign. This asymmetric peak can be interpolated by two peaks placed at −2.94 ppm (signal 44.3%) and +15.03 ppm (signal 50.1%). The peak at −2.94 ppm could overlap that of AlB_2 signal (+2.84 ppm), but, as confirmed by XRD analysis, its formation could not be detected up to 400 °C.

Composite-pulse decoupling (CPD) is a very useful technique to distinguish among species that contain B–H bonded atoms [37]. In the spectrum acquired without decoupling the proton (red line), a decrease of the signal relative to the B–H unit is observed in the peak centered at −2.94 ppm. This proves that the boron based specie associated to the signal at −2.94 ppm contains hydrogen. In addition, it is worth to claim that Al atoms is contained within this phase because during heating, the Al XRD peaks decrease drastically their intensity leading to the formation of the unknown phase. However, no ^{27}Al signal which could be associated to that phase is observed in Fig. 4B. The peak at +15.03 ppm is not influenced by decoupling proton, probably because contains B atoms which are not bonded to hydrogen. On the basis of ^{11}B MAS NMR studies in the literature, this resonance could be assigned to amorphous boron (+18 ppm) [36]. Summarizing, the *in situ* XRD and MAS NMR results suggest that the unknown phase is mainly composed by Li–Al–B–H atoms and, together with metal Al and amorphous boron, it represents a crucial intermediate in the decomposition mechanism of the $LiBH_4 + LiAlH_4$ system. Nevertheless, more efforts are still required in order to definitely clarify its chemical nature and its influence on the reversibility of the system.

4. Conclusions

In this work, we investigated the thermal decomposition of the $LiBH_4$–$LiAlH_4$ system. It is reported that the desorption of the 1:1 mixture reveals a multi-step reaction with a total weight loss of 6.8 wt.% of H_2 at 430 °C. In order to characterize the decomposition products evolved during heating, *in situ* SR-PXD experiment were performed. It is observed that the onset decomposition temperature of molten $LiBH_4$ takes place around 328 °C namely 50 °C less than pure $LiBH_4$. The molten $LiBH_4$ reacts with Al particles (produced by the decomposition of $LiAlH_4$ and Li_3AlH_6) forming an unidentified phase, already reported in the literature and releases hydrogen as confirmed by the variation of the pressure monitored during the *in situ* XRD experiments. As evinced by *ex situ* solid state MAS NMR, the unknown phase seems to be mainly composed by Li–B–Al–H atoms. This study represents a further progress in the full characterization of the reaction mechanism of the $LiBH_4$/Al-based system.

Acknowledgments

This work was funded by COST Action MP1103: "Nanostructured Materials for Solid State Hydrogen Storage", by MIUR (Italian Ministry for University and Research), in the frame of the PRIN Project "Synthesis, characterization and functional evaluation of light hydrides-based nanostructured materials and nanoparticles for solid state hydrogen storage", and by the University of Sassari. We thank the Serveis de Espectroscopia at UAB for their technical assistance and the beamline D3 in the research laboratory HASYLAB, DESY. This work has been supported by the 2009-SGR-1292 and MAT2010-20616-C02-02 of the Generalitat de Catalunya and the Spanish MINECO, respectively. M.D.B. acknowledges financial support from an ICREA-Academia Award.

References

[1] L. Schlapbach, A. Züttel, Hydrogen-storage materials for mobile applications, Nature 414 (2001) 353–358.
[2] S. Orimo, Y. Nakamori, J.R. Eliseo, A. Züttel, C.M. Jensen, Complex hydrides for hydrogen storage, Chem. Rev. 107 (2007) 4111–4132.
[3] J. Graetz, New approaches to hydrogen storage, Chem. Soc. Rev. 38 (2009) 73–82.
[4] M. Hirscher, Handbook of hydrogen storage: new materials for future energy storage, first ed., WILEY-VCH Verlag GmbH & Co. KGaA, Weinheim, 2010.
[5] W. Grochala, P.P. Edwards, Thermal decomposition of the non-interstitial hydrides for the storage and production of hydrogen, Chem. Rev. 104 (2004) 1283–1316.
[6] C. Li, P. Peng, D.W. Zhou, L. Wan, Research progress in $LiBH_4$ for hydrogen storage: a review, Int. J. Hydrogen Energy 36 (2011) 14512–14526.
[7] S. Orimo, Y. Nakamori, G. Kitahara, K. Miwa, N. Ohba, S. Towata, A. Züttel, Dehydriding and rehydriding reactions of $LiBH_4$, J. Alloys Comp. 404–406 (2005) 427–430.
[8] J. Yang, A. Sudik, C. Wolverton, Destabilizing $LiBH_4$ with a metal (M = Mg, Al, Ti, V, Cr, or Sc) of metal hydride (MH_2 = MgH_2, TiH_2, or CaH_2), J. Phys. Chem. C 111 (2007) 19134–19140.
[9] M. Au, A.R. Jurgensen, W.A. Spencer, D.L. Anton, F.E. Pinkerton, S.-J. Hwang, C. Kim, R.C. Bowman Jr., Stability and reversibility of lithium borohydrides doped by metal halides and hydrides, J. Phys. Chem. C 112 (2008) 18661–18671.
[10] X.B. Yu, D.M. Grant, G.S. Walker, Dehydrogenation of $LiBH_4$ destabilized with various oxides, J. Phys. Chem. C 113 (2009) 17945–17949.
[11] W. Cai, H. Wang, L. Jiao, Y. Wang, M. Zhu, Remarkable irreversible and reversible dehydrogenation of $LiBH_4$ by doping with nanosized cobalt metalloid compounds, Int. J. Hydrogen Energy 38 (2013) 3304–3312.
[12] F. Pendolino, P. Mauron, A. Borgschulte, A. Züttel, Effect of boron on the activation energy of the decomposition of $LiBH_4$, J. Phys. Chem. C 113 (2009) 17231–17234.
[13] P. Ngene, P. Adelhelm, A.M. Beale, K.P. de Jong, P.E. de Jongh, $LiBH_4$/SBA-15 nanocomposites prepared by melt infiltration under hydrogen pressure: synthesis and hydrogen sorption properties, J. Phys. Chem. C 114 (2010) 6163–6168.
[14] A.F. Gross, J.J. Vajo, S.L. Van Atta, G.L. Olson, Enhanced hydrogen storage kinetics of LiBH4 in nanoporous carbon scaffolds, J. Phys. Chem. C 112 (2008) 5651–5657.
[15] G. Capurso, F. Agresti, L. Crociani, G. Rossetto, B. Schiavo, A. Maddalena, S. Lo Russo, G. Principi, Nanoconfined mixed Li and Mg borohydrides as materials for solid state hydrogen storage, Int. J. Hydrogen Energy 37 (2012) 10768–10773.
[16] Z.-Z. Fang, X.-D. Kang, P. Wang, H.-M. Cheng, Improved reversible dehydrogenation of lithium borohydride by milling with as-prepared single-walled carbon nanotubes, J. Phys. Chem. C 112 (2008) 17023–17029.
[17] T.K. Nielsen, U. Bösenberg, R. Gosalawit, M. Dornheim, Y. Cerenius, F. Besenbacher, T.R. Jensen, A reversible nanoconfined chemical reaction, ACS Nano 4 (2010) 3903–3908.
[18] G. Barkhordarian, T. Klassen, M. Dornheim, R. Bormann, Unexpected kinetic effect of MgB_2 in reactive hydride composites containing complex borohydrides, J. Alloys Comp. 440 (2007) L18–L21.
[19] S. Garroni, C. Pistidda, M. Brunelli, G.B.M. Vaughan, S. Suriñach, M.D. Baró, Hydrogen desorption mechanism of $2NaBH_4 + MgH_2$ composite prepared by high-energy ball milling, Scr. Mater. 60 (2009) 1129–1132.
[20] S. Garroni, C. Milanese, A. Girella, A. Marini, G. Mulas, E. Menéndez, C. Pistidda, M. Dornheim, S. Suriñach, M.D. Baró, Sorption properties of $NaBH_4$/MH_2 (M = Mg, Ti) powder systems, Int. J. Hydrogen Energy 35 (2010) 5434–5441.
[21] C. Milanese, S. Garroni, A. Girella, G. Mulas, V. Berbenni, G. Bruni, S. Suriñach, M.D. Baró, A. Marini, Thermodynamic and kinetic investigations on pure and doped $NaBH_4$–MgH_2 system, J. Phys. Chem. C 115 (2011) 3151–3162.
[22] C. Pistidda, S. Garroni, C.B. Minella, F. Dolci, T.R. Jensen, P. Nolis, U. Bösenberg, Y Cerenius, W. Lohstroh, M. Fichtner, M.D. Baró, R. Bormann, M. Dornheim, Pressure effect on the $2NaH + MgB_2$ hydrogen absorption reaction, J. Phys.Chem.C 114 (2010) 21816–21823.
[23] C. Bonatto Minella, C. Pistidda, S. Garroni, P. Nolis, M.D. Baró, O. Gutfleisch, T. Klassen, R. Bormann, M. Dornheim, $Ca(BH_4)_2 + MgH_2$: desorption reaction and role of Mg on its reversibility, J. Phys. Chem. C 117 (2013) 3846–3852.
[24] U. Bösenberg, S. Doppiu, L. Mosegaard, G. Barkhordarian, N. Eigen, A. Borgschulte, T.R. Jensen, Y. Cerenius, O. Gutfleisch, T. Klassen, M. Dornheim, R. Bormann, Hydrogen sorption properties of MgH_2–$LiBH_4$ composites, Acta Mater. 55 (2007) 3951–3958.
[25] S.-A. Jin, J.-H. Shim, Y.W. Cho, K.-W. Yi, O. Zabara, M. Fichtner, Reversible hydrogen storage in $LiBH_4$–Al–LiH composite powder, Scr. Mater. 58 (2008) 963–965.
[26] J.F. Mao, Z.P. Guo, H.K. Liu, X.B. Yu, Reversible hydrogen storage in titanium-catalyzed $LiAlH_4$–$LiBH_4$ system, J. Alloys Comp. 487 (2009) 434–438.
[27] M. Meggouh, D.M. Grant, G.S. Walker, Optimizing the destabilization of $LiBH_4$ for hydrogen storage and the effect of different Al sources, J. Phys. Chem. C 115 (2011) 22054–22061.
[28] http://www.esrf.eu/computing/scientific/FIT2D/.
[29] P. Scardi, L. Lutterotti, P. Maistrelli, Experimental determination of the instrumental broadening in the Bragg–Brentano geometry, Powder Diffr. 9 (1994) 180–186.
[30] P.A. Amama, J.T. Grant, P.J. Shamberger, A.A. Voevodin, T.S. Fisher, Improved dehydrogenation properties of Ti-doped $LiAlH_4$: role of Ti precursors, J. Phys. Chem. C 116 (2012) 21886–21894.
[31] R.A Varin, T. Czujko, Z.S. Wronski, Nanomaterials for Solid State Hydrogen Storage, Springer, 2008, pp. 213–222.
[32] H.W. Brinks, B.C. Hauback, P. Norby, H. Fjellvag, The decomposition of $LiAlD_4$ studied by in situ X-ray and neutron diffraction, J. Alloys Comp. 351 (2003) 222–227.
[33] A. Züttel, S. Rentsch, P. Fischer, P. Wenger, P. Sudan, Ph. Mauron, Ch. Emmenegger, Hydrogen storage properties of $LiBH_4$, J. Alloys Comp. 356 (2003) 515–520.
[34] D.B. Ravnsbæk, T.R. Jensen, Mechanism for reversible hydrogen storage in $LiBH_4$–Al, J. Appl. Phys. 111 (2012) 112621–112629.
[35] B.R.S. Hansen, D.B. Ravnsbæk, D. Reed, D. Book, C. Gundlach, J. Skibsted, T.R. Jensen, Hydrogen storage capacity loss in a $LiBH_4$–Al composite, J. Phys. Chem. C 117 (2013) 7423–7432.
[36] Y.J. Choi, J. Lu, H.Y. Sohn, Z.Z. Fang, C. Kim, R.C. Bowman Jr., S.-J. Hwang, Reaction mechanisms in the Li_3AlH_6/$LiBH_4$ and Al/$LiBH_4$ systems for reversible hydrogen storage. Part 2: solid-State NMR studies, J. Phys. Chem. C 115 (2011) 6048–6056.
[37] S. Garroni, C. Milanese, D. Pottmaier, G. Mulas, P. Nolis, A. Girella, R. Caputo, D. Olid, F. Teixidor, M. Baricco, A. Marini, S. Suriñach, M.D. Baró, Experimental evidence of $Na_2[B_{12}H_{12}]$ and Na formation in the desorption pathway of the $2NaBH_4 + MgH_2$ system, J. Phys. Chem. C 115 (2011) 16664–16671.